Available online at www.sciencedirect.com
ScienceDirect
Journal of Computational Physics 222 (2007) 332–352
JOURNAL OF COMPUTATIONAL PHYSICS
www.elsevier.com/locate/jcp

Third-order-accurate fluctuation splitting schemes for unsteady hyperbolic problems

G. Rossiello, P. De Palma *, G. Pascazio, M. Napolitano

Dipartimento di Ingegneria Meccanica e Gestionale, Centro di Eccellenza in Meccanica Computazionale, Politecnico di Bari, Via Re David 200, 70125 Bari, Italy

Received 16 March 2006; received in revised form 26 June 2006; accepted 27 July 2006
Available online 11 September 2006

Abstract

This paper provides a two-dimensional fluctuation splitting scheme for unsteady hyperbolic problems which achieves third-order accuracy in both space and time. For a scalar conservation law, the sufficient conditions for a stable fluctuation splitting scheme to achieve a prescribed order of accuracy in both space and time are derived. Then, using a quadratic space approximation of the solution over each triangular element, based on the reconstruction of the gradient at the three vertices, and a four-level backward discretization of the time derivative, an implicit third-order-accurate scheme is designed. Such a scheme is extended to the Euler system and is validated versus well-known scalar-advection problems and inviscid discontinuous flows.

Keywords: Residual distribution; Unsteady Euler equations; Higher-order accuracy

1. Introduction

Fluctuation splitting (FS) schemes using a compact stencil have been developed and applied successfully for the last 15 years to compute a wide range of compressible steady flows with shocks [1–9]. The FS (also called residual distribution) approach is based on a cell-vertex tessellation of the computational domain and on a continuous reconstruction of the solution over linear (triangular/tetrahedral) elements. Only recently, the properties of these schemes have been studied also on quadrilateral meshes [10,11]. The method is based on three fundamental steps: (i) evaluating the residual, namely, the flux balance over each computational cell; (ii) distributing the residual contributions (signals) among the vertices of the cell using suitable coefficients; (iii) updating the solution at each node by summing up all contributions from the triangles sharing that node. More recently, attention has been paid to generalizing FS schemes to unsteady flows, a non-trivial task, insofar as a consistent mass matrix is needed to achieve an order of accuracy higher than one. Several approaches

* Corresponding author. Tel.: +39 0805963226; fax: +39 0805963411.
E-mail addresses: g.rossiello@poliba.it (G. Rossiello), depalma@poliba.it (P. De Palma), pascazio@poliba.it (G. Pascazio), napolita@poliba.it (M. Napolitano).

0021-9991/$ - see front matter
doi:10.1016/j.jcp.2006.07.027

have been pursued by different research groups to design second-order-accurate FS schemes [12–16]. Ferrante and Deconinck [13] employed a flux-corrected transport (FCT) procedure [17] applied to the triangle signals in combination with a Crank–Nicolson time integration. More recently, Csík et al. [15] and Abgrall and Mezine [16] proposed two implicit approaches in the framework of space–time residual-distribution schemes, extending non-linear FS schemes to continuous space–time elements. Such schemes are successful in eliminating spurious oscillations but cannot drive the residual to machine-zero in the iterative procedure. In Ref. [18], the authors provided an alternative implicit scheme based on a dual-time-stepping procedure and a general formulation of the consistent mass matrix, using a new limiting procedure to achieve monotone solutions. Such a procedure is similar to the FCT one, insofar as it allows to control the solution locally, so as to avoid the creation of spurious extrema; more importantly, it is employed at each node, after collecting the residual contributions from the neighboring elements, rather than at each triangle. In this way, the limiting procedure does not prevent the residual from reaching machine-zero (a feature which is fundamental for the use of any iterative solver) and may be employed in conjunction with any residual distribution scheme. On the other hand, with respect to the non-linear schemes of [15,16], this FCT-like approach needs the evaluation of two solutions (lower-order and higher-order ones) at each time step.

The aim of the present work is to provide a stable FS scheme with third-order accuracy in space and time, a goal which is being pursued also by other research groups. The basic step to increase the order of accuracy in space beyond two is to increase the degree of the solution approximation over each element (which is linear for a second-order-accurate scheme). This can be achieved following two strategies: (i) employing more general Lagrangian elements with a higher number of degrees of freedom (more than three), as proposed in [19,20]; (ii) reconstructing the gradient of the solution at the three vertices of each element using the value at the surrounding cells [21,22]. Concerning the time accuracy, one can either reconstruct the solution in space and time [19,20] or discretize the time derivative by suitable finite differences and then integrate it in space [21,22,18]. The sufficient conditions for an FS scheme to be $(r+1)$th-order accurate in the case of steady problems have been derived in [19]. On the other hand, for unsteady problems various error estimates have been provided in the recent literature, without any rigorous proof, which are inconsistent [16,23,20]. Therefore, in this paper, the procedure proposed in [19] for steady problems is generalized to unsteady ones so as to provide the correct sufficient conditions for the accuracy of an FS scheme to achieve order $(r+1)$ in space and time, in the case of a finite difference discretization of the time derivative as well as in the case of a space–time approach. Then, a third-order-accurate scheme is proposed, in which the desired space accuracy is achieved by reconstructing the gradient of the solution at the vertices of each element and the time one is obtained by an implicit scheme employing a four-point backward finite difference formula. Such a scheme is validated versus well-known scalar-advection problems. Then, it is extended to the solution of the Euler equations and applied successfully to compute unsteady inviscid flows with or without discontinuities. Finally, a weak formulation of FS schemes is provided in the appendix, which shows how such schemes can be recovered within the finite-element framework.

2. Scalar advection

Consider the two-dimensional scalar conservation law:

$$\frac{\partial u}{\partial t} + \nabla \cdot \mathbf{F} = 0 \tag{1}$$

with $u : \Theta \to \mathbb{R}$, $\Theta = \Omega \times [0, +\infty[$, $\Omega \subseteq \mathbb{R}^2$, $\mathbf{F} = (f(u), g(u))^{\mathscr{T}}$. For linear advection, the flux vector can be expressed as $\mathbf{F} = \boldsymbol{\lambda} u$, where $\boldsymbol{\lambda} = (a, b)^{\mathscr{T}}$ is the advection velocity. For a divergence-free advection velocity, Eq. (1) governs the advection of a scalar quantity.

2.1. Fluctuation splitting schemes

The spacial computational domain, Ω, is divided into cell-vertex triangular elements, T, the generic node being labeled i, and time is discretized into levels, labeled n, with increment Δt. For the steady case, explicit FS schemes are obtained by three main steps:

(i) evaluating the fluctuation, ϕ^T, namely, the flux balance over the cell:

$$\phi^{T,n} = \int_T \nabla \cdot \mathbf{F}(u^n)\,\mathrm{d}\Omega; \tag{2}$$

(ii) distributing the fluctuation among the nodes j of each triangle:

$$\phi_j^{T,n} = (\beta_j^T \phi^T)^n \quad \text{with} \quad \sum_{j\in T} \beta_j^{T,n} = 1, \tag{3}$$

where $\phi_j^{T,n}$ is the *signal* from triangle T to node j;

(iii) updating the solution at each node i by summing up all contributions from the triangles sharing that node:

$$u_i^{n+1} = u_i^n - \frac{\Delta t}{|S_i|} \sum_{T\ni i} \phi_i^{T,n}, \tag{4}$$

where $|S_i|$ is the area of the dual-cell, S_i. In Appendix A a derivation of the FS discretization from the weak formulation of Eq. (1) is provided. The first two steps, namely, the residual evaluation and distribution, are essential for the accuracy of the scheme at steady state. Assuming that the unknown varies linearly over each cell, the discrete fluctuation can be evaluated as:

$$\phi^T = -\sum_{j=1}^{3} k_j u_j, \quad k_j = \frac{1}{2}\boldsymbol{\lambda}\cdot\boldsymbol{n}_j \ell_j, \tag{5}$$

$\boldsymbol{n}_j$ and ℓ_j being the inward unit normal to the edge opposing node j and its length, respectively. Distributing such a fluctuation using bounded coefficients, β_j^T, a Linearity Preserving ($\mathscr{LP}$) scheme is obtained, namely, a scheme which preserves an initial exact linear solution, thus being second-order accurate in space for homogeneous advection equations [24]. Several FS schemes have been designed, the final goal being a monotone and second-order-accurate scheme, an impossible task for any linear scheme [1]. Most of such schemes are of the (multi-dimensional) upwind type, namely, they are obtained by assigning to each downstream node j, $k_j \geqslant 0$, a fraction β_j^T of the cell fluctuation. In the trivial configuration of Fig. 1a, the entire fluctuation is assigned to the only downstream node and the resulting FS scheme is both positive and second-order accurate. For the non-trivial configuration of Fig. 1b, different choices of the distribution coefficients β_j^T characterize the different schemes.

For the present study, the following FS schemes are of interest: (1) the N scheme, which is the optimal first-order-accurate upwind scheme [1]:

$$\phi_j^N = -k_j^+(u_j - u_{\mathrm{in}}), \quad u_{\mathrm{in}} = \frac{\sum_{j=1}^3 k_j^- u_j}{\sum_{j=1}^3 k_j^-}, \tag{6}$$

where $k_j^+ = \max(0, k_j)$ and $k_j^- = \min(0, k_j)$.

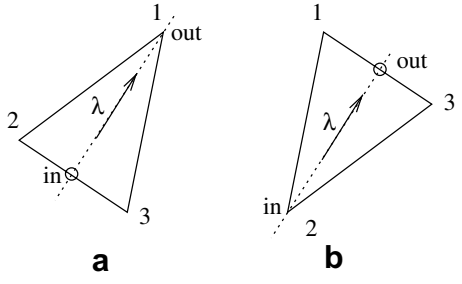

Fig. 1. Definition of inflow and outflow points: (a) One target case, and (b) two target case.

(2) The non-upwind FS Lax–Wendroff (LW) scheme [24]:

$$\phi_j^{\mathrm{LW}} = \left(\frac{1}{3} + \frac{\Delta t}{2|T|} k_j\right) \phi^T = \beta_{T,j}^{\mathrm{LW}} \phi^T, \tag{7}$$

where $|T|$ is the area of triangle T. Such an explicit scheme achieves second-order accuracy in space and time [14].

(3) The second-order-accurate upwind control volume (UCV) scheme [24]:

$$\phi_j^{\mathrm{UCV}} = \left(\frac{1}{3} + \frac{2}{3} \frac{k_j}{\sum_{i=1}^{3} |k_i|}\right) \phi^T = \beta_{T,j}^{\mathrm{UCV}} \phi^T. \tag{8}$$

2.2. Accuracy conditions for FS schemes

In this section, the analysis provided in [19] for a steady equation is recalled and then generalized to the case of an unsteady scalar conservation law, to determine the sufficient conditions for an FS scheme to provide a truncation error of $\mathcal{O}(h^{r+1})$ in both space and time. In particular, two approaches are analyzed using either a space–time discretization or a backward finite-difference formula for the time derivative. Consider the following partial differential equation defined in the d dimensional domain Ω:

$$\mathscr{L}(u) = 0, \tag{9}$$

with the corresponding weak form:

$$\int_\Omega \varphi \mathscr{L}(u)\, \mathrm{d}\Omega = 0, \tag{10}$$

where $\varphi(\mathbf{x})$ is any $\mathscr{C}_{\mathbf{0}}^{\mathbf{1}}$ function with compact support in $\mathbb{R}^d$. Given an approximate tessellation of the domain, with linear dimension h, the numerical method can be written as follows: find u_i, $\forall \text{node}\, i \in \Omega$, such that

$$\int_\Omega \omega_i \mathscr{L}^h(u^h(u_j))\, \mathrm{d}\Omega = \sum_{E \ni i} \Phi_i^E(u_j) = 0, \tag{11}$$

where

$$\Phi_i^E(u_j) = \int_E \omega_i \mathscr{L}^h(u^h(u_j))\, \mathrm{d}\Omega, \tag{12}$$

ω_i being a weight function with compact support defining the scheme, the summation is extended to the elements sharing node i, and u^h is a polynomial representation based on the computed nodal values u_j, with $j \in E$.[1]

In order to evaluate the accuracy of the scheme, consider the polynomial representation of the exact solution of Eq. (10), $u^h = u^h(u_j^{\mathrm{ex}})$, so that the truncation error reads:

$$\mathrm{TE} = \left| \sum_i \varphi_i \sum_{E \ni i} \Phi_i^E - \int_\Omega \varphi \mathscr{L}(u)\, \mathrm{d}\Omega \right|, \tag{13}$$

where the second term vanishes since u indicates the exact solution. On the other hand, following [19], the first term can be written as:

$$\begin{aligned} \sum_i \varphi_i \sum_{E \ni i} \Phi_i^E &= \sum_i \sum_{E \ni i} \varphi_i \Phi_i^E = \sum_i \sum_{E \ni i} \varphi_i \Gamma_i^E + \sum_i \sum_{E \ni i} \varphi_i (\Phi_i^E - \Gamma_i^E) \\ &= \int_\Omega \varphi^h \mathscr{L}^h(u^h)\, \mathrm{d}\Omega + \sum_i \sum_{E \ni i} \varphi_i (\Phi_i^E - \Gamma_i^E). \end{aligned} \tag{14}$$

[1] Notice that u_j can be either the values of the degrees of freedom in the element or interpolated values using degrees of freedom from surrounding elements.

In the equation above, the following definitions have been used:

$$\varphi^h = \sum_i \varphi_i \psi_i, \tag{15}$$

$$\Gamma_i^E = \int_E \psi_i \mathscr{L}^h(u^h)\,\mathrm{d}\Omega, \tag{16}$$

where ψ_i is the Lagrangian basis function of degree r.

Consider the case of a steady conservation equation:

$$\mathscr{L}(u) = \nabla \cdot \mathbf{F}(u) = 0, \tag{17}$$

where $u : \Omega \rightarrow \mathbb{R}$, with $\Omega \subseteq \mathbb{R}^d$.

According to Eq. (11), the scheme reads:

$$\int_\Omega \omega_i \nabla \cdot \mathbf{F}^h(u^h(u_j))\,\mathrm{d}\Omega = \sum_{T \ni i} \phi_i^T(u_j) = 0. \tag{18}$$

For an $(r+1)$th-order-accurate approximation $\mathbf{F}^h$ of $\mathbf{F}$, the first term on the right-hand side of Eq. (14) can be integrated by parts to give

$$\int_\Omega \varphi^h \nabla \cdot \mathbf{F}^h(u^h)\,\mathrm{d}\Omega = \int_{\partial\Omega} \varphi^h(\mathbf{F}^h(u^h) - \mathbf{F}(u)) \cdot \mathbf{n}\,\mathrm{d}\ell - \int_\Omega \nabla\varphi^h \cdot (\mathbf{F}^h(u^h) - \mathbf{F}(u))\,\mathrm{d}\Omega = \mathscr{O}(h^{r+1}). \tag{19}$$

The second term on the right-hand side of Eq. (14) can be arranged as follows:

$$\begin{aligned}\sum_i \sum_{T \ni i} \varphi_i(\phi_i^T - \Gamma_i^T) &= \sum_T \sum_{i \in T} \varphi_i(\phi_i^T - \Gamma_i^T) = \sum_T \sum_{i \in T} (\varphi_i - \varphi^*)(\phi_i^T - \Gamma_i^T) \\ &= \sum_T \sum_{i \in T} (\varphi_i - \varphi^*)\phi_i^T - \sum_T \sum_{i \in T} (\varphi_i - \varphi^*)\Gamma_i^T\end{aligned} \tag{20}$$

where φ^* indicates the value of φ in an arbitrary point of triangle T. In Eq. (20), the following equivalence has been used:

$$\sum_{i \in T} \phi_i^T = \sum_{i \in T} \Gamma_i^T. \tag{21}$$

Thanks to the above assumption on $\mathbf{F}^h$ and integrating by parts over the element, like for Eq. (19), one has:

$$\Gamma_i^T = \int_T \psi_i \nabla \cdot \mathbf{F}^h(u^h)\,\mathrm{d}\Omega = \int_{\partial T} \psi_i(\mathbf{F}^h(u^h) - \mathbf{F}(u)) \cdot \mathbf{n}\,\mathrm{d}\ell - \int_T \nabla\psi_i \cdot (\mathbf{F}^h(u^h) - \mathbf{F}(u))\,\mathrm{d}\Omega = \mathscr{O}(h^{r+d}). \tag{22}$$

Since the number of elements is $\mathscr{O}(h^{-d})$ and

$$\varphi_i - \varphi^* = \mathscr{O}(h), \tag{23}$$

it turns out that:

$$\sum_T \sum_{i \in T} (\varphi_i - \varphi^*)\Gamma_i^T = \mathscr{O}(h^{r+1}). \tag{24}$$

Therefore, from Eq. (20), if $\phi_i^T = \mathscr{O}(h^{r+d})$, then

$$\sum_i \sum_{T \ni i} \varphi_i(\phi_i^T - \Gamma_i^T) = \mathscr{O}(h^{r+1}). \tag{25}$$

In conclusion, the truncation error is $\mathscr{O}(h^{r+1})$ if an $(r+1)$th-order-accurate approximation $\mathbf{F}^h$ is used and if $\phi_i^T = \mathscr{O}(h^{r+d})$; the latter condition on the signals can be fulfilled provided that a suitable approximation of the space integral is employed for computing the fluctuation and bounded distribution functions are used.

The analysis above, due to [19], can be extended to a space–time approach by defining

$$\mathscr{L}(u) = \frac{\partial u}{\partial t} + \nabla \cdot \mathbf{F}(u) = \nabla_t \cdot \mathbf{G}(u) = 0, \tag{26}$$

with $\nabla_t = \frac{\partial}{\partial t}\mathbf{t} + \nabla$ and $\mathbf{G} = (u, \mathbf{F})^T$, and writing Eq. (11) as

$$\int_\Theta \omega_i \mathscr{L}^h(u^h(u_j))\,\mathrm{d}\Theta = \int_0^{+\infty}\int_\Omega \omega_i \mathscr{L}^h(u^h(u_j))\,\mathrm{d}\Omega\,\mathrm{d}t = \sum_{E\ni i} \Phi_i^E(u_j) = 0, \tag{27}$$

where E and Φ_i^E indicate the space–time elements and signals, respectively, and h is the linear measure of E. All of the steps taken in Eqs. (14)–(25) can be carried out again with the above definitions, leading to the following conclusion: the truncation error is $\mathcal{O}(h^{r+1})$ if an $(r+1)$th-order-accurate approximation $\mathbf{G}^h$ of $\mathbf{G}$ is used and if $\Phi_i^E = \mathcal{O}(h^{r+d+1})$. The latter condition on the signals can be fulfilled provided that a suitable approximation of the space–time integrals is employed for computing the fluctuation and bounded distribution functions are used. Notice that the requirement on the signals for $(r+1)$ accuracy in space–time is one order higher than that for the steady case, since the integration is now performed in the $d+1$ domain, see Eq. (27). On the other hand, the condition on the degree of the polynomial interpolation $u^h(\mathbf{x}, t)$ remains r in both space and time.

Consider now

$$\mathscr{L}(u) = \frac{\partial u}{\partial t} + \nabla\cdot\mathbf{F}(u) = 0 \tag{28}$$

with a discretization of the time derivative using a backward multi-step scheme. Eq. (11) gives

$$\int_\Omega \omega_i\left(\frac{\partial u^h(u_j)}{\partial t} + \nabla\cdot\mathbf{F}^h(u^h(u_j))\right)\mathrm{d}\Omega = \sum_{T\ni i}\Phi_i^T(u_j) = 0, \tag{29}$$

where both terms in the integral must be computed at the same time level, leading in general to an implicit scheme.

The accuracy conditions are derived again from Eq. (14) where the integration (and distribution) has to be considered only over the space domain. Therefore, using a constant Δt, proportional to the spacial grid-size h, the first term on the right-hand side of Eq. (14) reads:

$$\begin{aligned}\int_\Omega \varphi^h \nabla\cdot\mathbf{F}^h(u^h)\,\mathrm{d}\Omega + \int_\Omega \varphi^h\frac{\partial u^h}{\partial t}\mathrm{d}\Omega &= \int_{\partial\Omega}\varphi^h(\mathbf{F}^h(u^h)-\mathbf{F}(u))\cdot\mathbf{n}\,\mathrm{d}\ell - \int_\Omega \nabla\varphi^h\cdot(\mathbf{F}^h(u^h)-\mathbf{F}(u))\,\mathrm{d}\Omega\\ &\quad + \int_\Omega \varphi^h\left(\frac{\partial u^h}{\partial t} - \frac{\partial u}{\partial t}\right)\mathrm{d}\Omega = \mathcal{O}(h^{r+1});\end{aligned} \tag{30}$$

this result comes from Eq. (19) provided that a reconstruction is used which is $(r+1)$th-order-accurate in time for $\partial u^h/\partial t$ and $(r+1)$th-order-accurate in space for u^h. Notice that this conditions are needed in addition to the one required for $\mathbf{F}^h$.

The second term on the right-hand side of Eq. (14) can be written again as in Eq. (20) where, according to Eq. (16),

$$\begin{aligned}\Gamma_i^T &= \int_T \psi_i\left[\nabla\cdot\mathbf{F}^h(u^h) + \frac{\partial u^h}{\partial t}\right]\mathrm{d}\Omega\\ &= \int_{\partial T}\psi_i(\mathbf{F}^h(u^h)-\mathbf{F}(u))\cdot\mathbf{n}\,\mathrm{d}\ell - \int_T \nabla\psi_i\cdot(\mathbf{F}^h(u^h)-\mathbf{F}(u))\,\mathrm{d}\Omega + \int_T\psi_i\left(\frac{\partial u^h}{\partial t}-\frac{\partial u}{\partial t}\right)\mathrm{d}\Omega.\end{aligned} \tag{31}$$

In the equation above, the first two terms on the right-hand side are $\mathcal{O}(h^{r+d})$ like for Eq. (22), whereas the last term is $\mathcal{O}(h^{r+d+1})$ due to the assumption on the time derivative approximation. Therefore,

$$\Gamma_i^T = \mathcal{O}(h^{r+d}) \tag{32}$$

and

$$\sum_i\sum_{T\ni i}\varphi_i(\Phi_i^T - \Gamma_i^T) = \mathcal{O}(h^{r+1})$$

provided that $\Phi_i^T = \mathcal{O}(h^{r+d})$. In conclusion, for the case of the unsteady advection equation, the truncation error is $\mathcal{O}(h^{r+1})$ if: an $(r+1)$th-order-accurate space reconstruction is used for $\mathbf{F}^h$ and u^h; an $(r+1)$th-order-accurate

finite difference discretization in time is employed for $(\partial u/\partial t)_i$; and $\Phi_i^T = \mathcal{O}(h^{r+d})$. The latter condition on the signals can be fulfilled provided that a suitable approximation of the space integrals of both the unsteady and steady terms is employed for computing the fluctuation and bounded distribution functions are used. In general, the signals are to be computed implicitly.

It is noteworthy that the above analysis can be extended straightforwardly to the case of an advection equation with a source term [25], whose treatment and accuracy requirements are similar to those of the time derivative.

2.3. Steady problems

2.3.1. Third-order-accurate FS schemes

The analysis described above allows one to design higher-order-accurate space-discretization schemes, using a cell-residual evaluation based on a higher-degree polynomial reconstruction and a distribution step with bounded coefficients. The following conditions are sufficient for an FS scheme to achieve third-order accuracy at steady state for smooth solutions on a grid with spacing h in two dimensions ($d = 2$, $r = 2$):

R1: the fluctuation over each triangle T needs to be computed such that

$$\phi^T = \int_T \nabla \cdot \mathbf{F}^h(u^h)\,\mathrm{d}\Omega = -\int_{\partial T} \mathbf{F}^h(u^h)\cdot \mathbf{n}\,\mathrm{d}\ell = 0 + \mathcal{O}(h^4),$$

$\mathbf{n}$ being the inward unit vector normal to the edges of T.

R2: the distribution coefficients, β_i^T, must be bounded, so that, because of R1, $\phi_i^T = \beta_i^T \phi^T = 0 + \mathcal{O}(h^4)$.

Condition R2 can be satisfied using *classical* FS schemes with bounded coefficients, such as the previously shown LW and UCV ones [24]. Condition R1 can be fulfilled via a quadratic polynomial reconstruction of u and a contour integration using only cell-vertex values, the mid-point values on each edge being evaluated by a reconstruction involving the neighboring cells [21,22]. To this purpose, the gradient of the solution at each vertex is employed (superscript h is omitted for brevity):

$$\nabla u_i = \frac{1}{\sum\limits_{T\ni i} |T|^{-1}} \sum_{T\ni i} |T|^{-1} \nabla u_T, \tag{33}$$

where the gradient over each element is evaluated as:

$$\nabla u_T = \frac{1}{2|T|} \sum_{j=1}^{3} u_j \boldsymbol{n}_j \ell_j. \tag{34}$$

The parabolic function along the edge can thus be defined, allowing one to evaluate the sought mid-point value as:

$$u_{\mathrm{mid},j} = \frac{u_m + u_p}{2} + \frac{\nabla u_m - \nabla u_p}{8}\cdot(\boldsymbol{x}_p - \boldsymbol{x}_m), \tag{35}$$

where $m = (j-1) \bmod 3$ and $p = (j+1) \bmod 3$. The same formula was derived in Ref. [21] using a least-square-fitting technique.

The fluctuation is computed using the Simpson formula on each edge; for the case of constant advection velocity, one has:

$$\phi^T = -\sum_{j=1}^{3} \frac{\boldsymbol{\lambda}\cdot \boldsymbol{n}_j \ell_j}{6}[u_m + 4u_{\mathrm{mid},j} + u_p]. \tag{36}$$

In the present study, all computations have been performed using uniform Cartesian grids, the quadrilateral cells being divided into two triangles by alternating diagonals.

2.3.2. Steady linear advection of a cosine-shaped function

The numerical accuracy of each scheme has been verified by computing the steady linear advection of a cosine-shaped function with advection velocity $\boldsymbol{\lambda} = (2, 1)$ in the $[0, 1] \times [0, 2]$ domain with periodic boundary conditions, corresponding to the exact solution $u = \cos[\pi(x - 2y)]$. Fig. 2 provides a mesh-refinement study using a sequence of five grids starting from $h = \Delta x = \Delta y = 1/10$. The results obtained using the UCV distribution coefficients in conjunction with the present third-order-accurate scheme (FS3) are shown, together with those of the second-order-accurate scheme (FS2) employing a linear reconstruction of the solution. The third-order-accurate scheme provides fourth-order convergence for both the L_1 and L_∞ error-norms, due to a well-known cancellation property of the Simpson integration formula (36), which integrates exactly polynomials of degree three.

2.4. Unsteady problems

2.4.1. Third-order-accurate FS schemes

For the case of unsteady problems, an implicit scheme based on a dual-time-stepping technique [26] is employed:

$$u_i^{n+1,k+1} = u_i^{n+1,k} - \frac{\Delta\tau}{|S_i|}\sum_{T\ni i}(\alpha_i^T\zeta^T + \beta_i^T\phi^T)^{n+1,k} = u_i^{n+1,k} - \frac{\Delta\tau}{|S_i|}\sum_{T\ni i}(\zeta_i^T + \phi_i^T)^{n+1,k}, \tag{37}$$

where the explicit Euler integration is used in the dual time τ, the superscripts n and k indicate the physical and fictitious time levels, respectively, and

$$\zeta^T = \int_T \frac{\partial u}{\partial t}\mathrm{d}\Omega, \tag{38}$$

is the unsteady residual. At each new physical time level $n + 1$, Eq. (37) is iterated until the solutions at pseudo-time levels $k + 1$ and k coincide within a prescribed tolerance. The time derivative is discretized by a back-

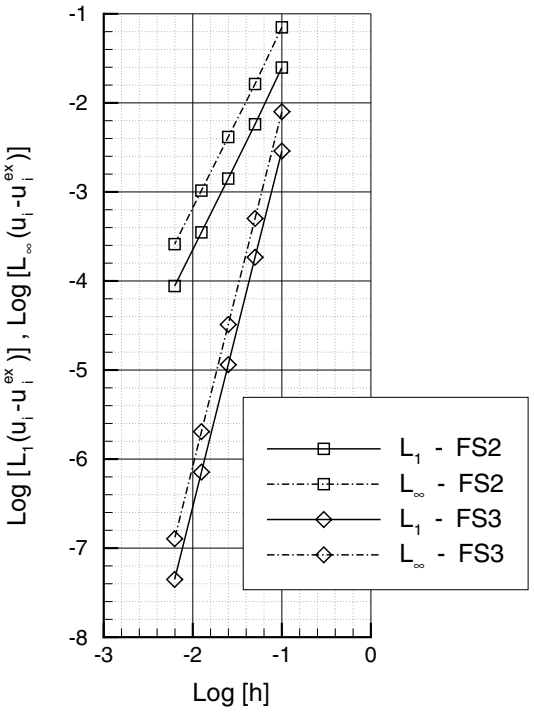

Fig. 2. Mesh-refinement study for the steady scalar problem: L_1 and L_∞ error-norms for the second- and third-order-accurate schemes.

ward finite-difference formula. In order to obtain a third-order-accurate scheme in space and time, the conclusions of Section 2.2 indicate the following sufficient conditions:

(1) compute the time derivative using a third-order-accurate backward four-level scheme:

$$\left(\frac{\partial u}{\partial t}\right)_i = \frac{11u_i^{n+1} - 18u_i^n + 9u_i^{n-1} - 2u_i^{n-2}}{6\Delta t}; \tag{39}$$

(2) employ a quadratic reconstruction of the solution over the cell so that the unsteady residual reads:

$$\zeta^T = \frac{|T|}{3}\sum_{j=1}^{3}\left(\frac{\partial u}{\partial t}\right)_{\mathrm{mid},j}; \tag{40}$$

(3) evaluate the steady residual, ϕ^T, using a quadratic reconstruction of the flux as described in the previous section;
(4) compute the signal so that $\Phi_i^T = \zeta_i^T + \phi_i^T = 0 + \mathcal{O}(h^4)$.

Considering the simplest choice of distributing the entire residual by means of the same scheme, namely, using bounded coefficients with $\alpha_i^T = \beta_i^T$ [21,22], condition (4) is satisfied but stability problems are experienced due to insufficient dissipation. Therefore, an alternative distribution procedure is provided here, which shows good stability properties, while maintaining third-order accuracy in both space and time. Consider a linear reconstruction ($r = 1$) of the numerical solution over each element, u_ℓ, and define u_q as the difference between the actual reconstruction of second degree and the linear one, $u_q = u - u_\ell$. The steady and unsteady residuals are split into two contributions, $\phi^T = \phi_\ell^T + \phi_q^T$ and $\zeta^T = \zeta_\ell^T + \zeta_q^T$, where ϕ_ℓ^T and ζ_ℓ^T are the fluctuations computed using u_ℓ, and ϕ_q^T and ζ_q^T are the higher-order corrections, namely,

$$\phi_q^T = \phi^T - \phi_\ell^T \quad \text{and} \quad \zeta_q^T = \zeta^T - \zeta_\ell^T. \tag{41}$$

Therefore, the fluctuation can be written as

$$\zeta^T + \phi^T = \zeta_\ell^T + \zeta_q^T + \phi_\ell^T + \phi_q^T. \tag{42}$$

It is noteworthy that ϕ_ℓ^T and ϕ_q^T are $\mathcal{O}(h^3)$, since, for a linear reconstruction of the solution, one has

$$\phi_\ell^T = \int_T \nabla\cdot\mathbf{F}(u_\ell)\,\mathrm{d}\Omega = -\int_{\partial T}\mathbf{F}(u_\ell)\cdot\mathbf{n}\,\mathrm{d}\ell = 0 + \mathcal{O}(h^3);$$

moreover, since $\phi^T = \mathcal{O}(h^4)$, it follows from Eq. (41) that $\phi_q^T = \mathcal{O}(h^3)$. This is confirmed by the numerical results shown in Fig. 3, which refer to the steady problem described in Section 2.3.2, where the steady fluctuation is seen to be $\mathcal{O}(h^5)$ instead of $\mathcal{O}(h^4)$ for the aforementioned property of Simpson's rule, in agreement with the results of Fig. 2. For a linear reconstruction of the solution in space, u_ℓ, one has:

$$\zeta_\ell^T + \phi_\ell^T = \int_T\left(\frac{\partial u_\ell}{\partial t} + \nabla\cdot\mathbf{F}(u_\ell)\right)\mathrm{d}\Omega = 0 + \mathcal{O}(h^3).$$

On the other hand, it can be easily demonstrated that $\zeta_q^T = \mathcal{O}(h^4)$. In fact, as already shown for the last term in the right-hand side of Eq. (31):

$$\int_T\left(\frac{\partial u^h}{\partial t} - \frac{\partial u}{\partial t}\right)\mathrm{d}\Omega = \int_T\left(\frac{\partial u_\ell^h}{\partial t} - \frac{\partial u}{\partial t}\right)\mathrm{d}\Omega + \int_T\frac{\partial u_q^h}{\partial t}\mathrm{d}\Omega = \mathcal{O}(h^5). \tag{43}$$

Since

$$\int_T\left(\frac{\partial u_\ell^h}{\partial t} - \frac{\partial u}{\partial t}\right)\mathrm{d}\Omega = \mathcal{O}(h^4), \tag{44}$$

from Eq. (43) it follows that:

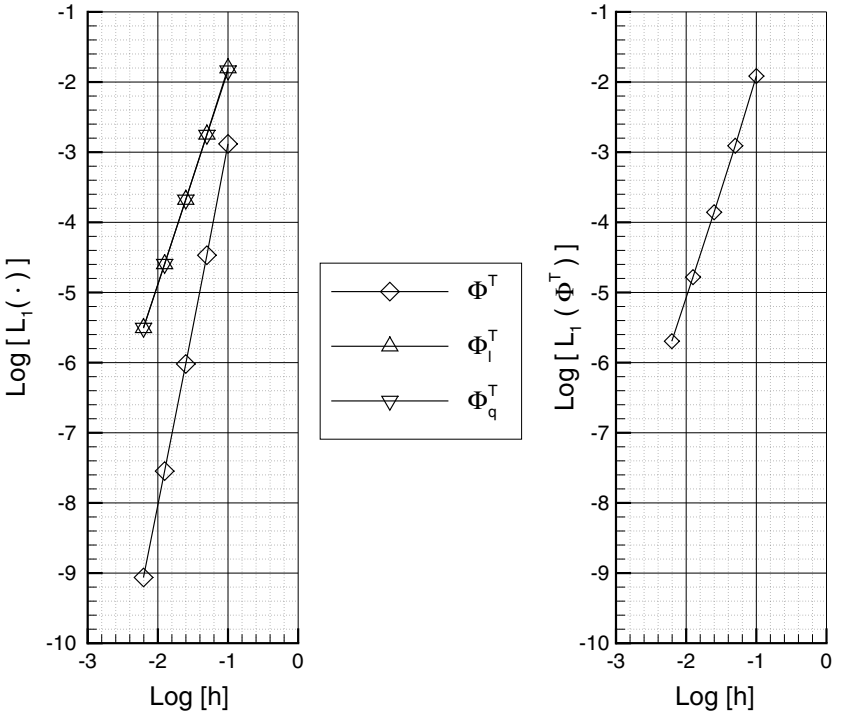

Fig. 3. Mesh-refinement study for the steady scalar problem: fluctuation accuracy for the third-order-accurate scheme (left) and the second-order-accurate scheme (right).

$$\zeta_q^T = \int_T \frac{\partial u_q^h}{\partial t} \mathrm{d}\Omega = \mathcal{O}(h^4). \tag{45}$$

Finally, the signals are evaluated as

$$\zeta_i^T + \phi_i^T = \beta_i^T (\zeta_\ell^T + \phi_\ell^T + \phi_q^T) + \frac{1}{3}\zeta_q^T. \tag{46}$$

A slightly increased numerical dissipation renders such a scheme stable and does not alter its order of accuracy, since the accuracy requirements are still fulfilled. The distribution coefficients, β_i^T, of the UCV scheme have been used to obtain the present numerical results; it is noteworthy that only negligible differences are observed using different $\mathscr{LP}$ distribution schemes. Notice that the proposed third-order-accurate scheme is different from the one provided in [21,22] in two points: (i) a third-order-accurate discretization of the time derivative is employed here instead of the second-order-accurate formula of [21,22]; (ii) the distribution step is performed according to Eq. (46). Finally, it is noteworthy that the cost of one iteration employing the proposed third-order-accurate scheme is 1.7 and 2.5 times greater than those of the second-order-accurate FS scheme and of the FS-LW one, respectively.

2.4.2. Accuracy study: advection of a double-sine function

The accuracy of the proposed scheme has been verified by computing the unsteady linear advection of a double-sine-shaped function (see Fig. 4),

$$u = \sin(2\pi x)\sin(2\pi y),$$

with $\boldsymbol{\lambda} = (1, 2)$, in the periodic domain $[0, 1]\times[0, 1]$ up to $t = 1$. Four different schemes have been used, namely:

(1) the explicit second-order-accurate FS Lax–Wendroff scheme (LW);

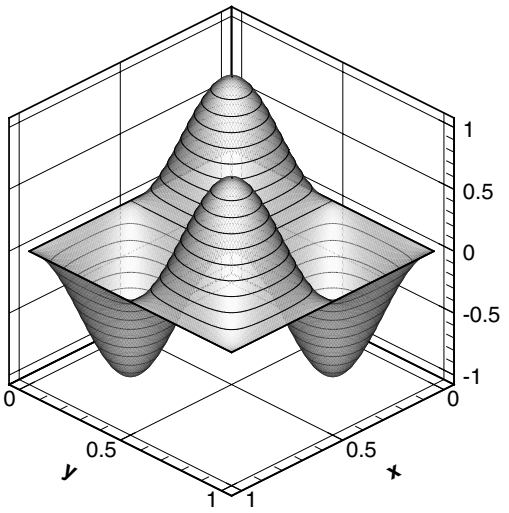

Fig. 4. Double-sine-shaped function for the unsteady scalar test case.

(2) the implicit second-order-accurate scheme, obtained by using a consistent mass matrix approach and the UCV scheme [18] (FS2);
(3) the implicit third-order-accurate scheme with $\alpha_i^T = \beta_i^T$, using the UCV distribution coefficients (FS3up);
(4) the implicit third-order-accurate scheme defined by Eq. (46), using the UCV distribution coefficients (FS3).

A sequence of five grids has been used, starting from $h = \Delta x = \Delta y = 1/16$ and $\Delta t = 0.02$, and halving both the space and time steps. It is noteworthy that, using the third-order-accurate schemes, about 10 inner iterations are needed to reduce the L_∞ norm of the residual to 10^{-10}. The L_1 and L_∞ norms of the errors are reported in Fig. 5, which confirm the accuracy of all schemes. Notice that the curve referring to the simple $\alpha_i^T = \beta_i^T$ scheme is truncated to the 128×128 grid, since instabilities arise when refining the mesh further, which forbid to obtain the numerical solution. Finally, Fig. 6 provides the accuracy of the fluctuations. The global fluctuation, $\zeta^T + \phi^T$, and the term ζ_q^T are $\mathcal{O}(h^4)$, whereas the linear fluctuation, $\zeta_\ell^T + \phi_\ell^T$, and the quadratic correction, ϕ_q^T, are only $\mathcal{O}(h^3)$, in perfect agreement with the previous theoretical findings.

2.4.3. Circular advection of a hump

The circular advection of a smooth hump

$$u = \begin{cases} \cos^2(2\pi r) & \text{for } r \leqslant 0.25 \\ 0 & \text{for } r > 0.25 \end{cases}, \quad r^2 = (x + 0.5)^2 + y^2,$$

in the square domain $[-1, 1]^2$ with $\boldsymbol{\lambda} = (-2\pi y, 2\pi x)$, is computed using a grid with $\Delta x = \Delta y = 1/32$ and $\Delta t = 0.0025$. The hump follows a circular path and returns to its initial position at $t = 1$.

Figs. 7–9 provide the solutions obtained using the linear and non-linear versions of the following three schemes: the Lax–Wendroff scheme (LW); the implicit second-order-accurate scheme (FS2) referred to as MM-CU in Ref. [18]; the implicit third-order-accurate scheme (FS3) of Eq. (46). The non-linear version of each scheme is obtained applying the limiting procedure described in Ref. [18], with the explicit N scheme providing the low-order solution at each step; no change is needed when applying the limiting procedure to the third-order scheme. It is noteworthy that, using either the linear or the non-linear third-order-accurate schemes, about 50 inner iterations are needed to reduce the L_∞ norm of the residual to 10^{-10}. The results provided in Figs. 7–9 clearly show the superior accuracy of the third-order-accurate schemes: the dispersion error is lower than that of the second-order-accurate implicit scheme. This appears more clearly from the vertical cuts through the exact centre of the hump (*i.e.*, $x = -0.5$):

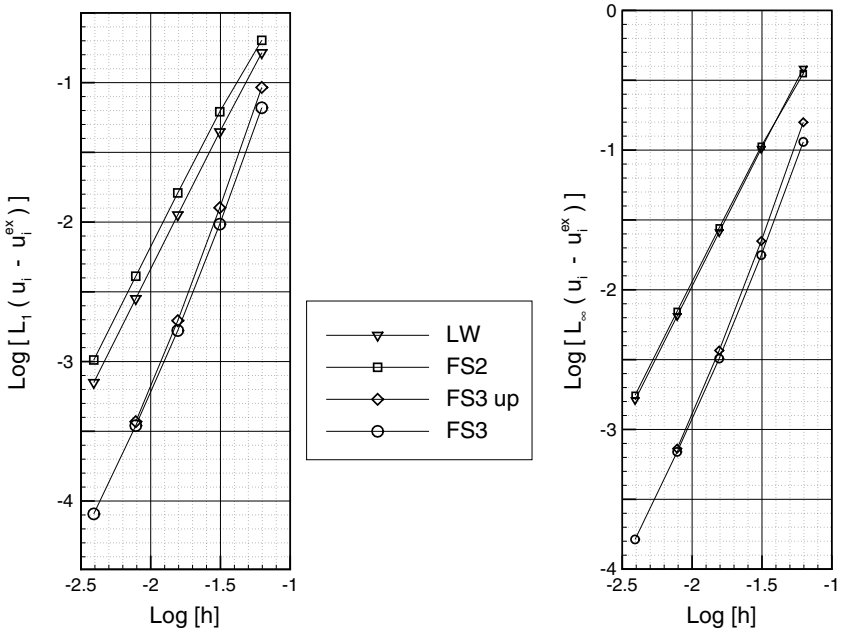

Fig. 5. Mesh-refinement study for the unsteady scalar problem: L_1 (left) and L_∞ (right) error-norms for the second- and third-order-accurate schemes.

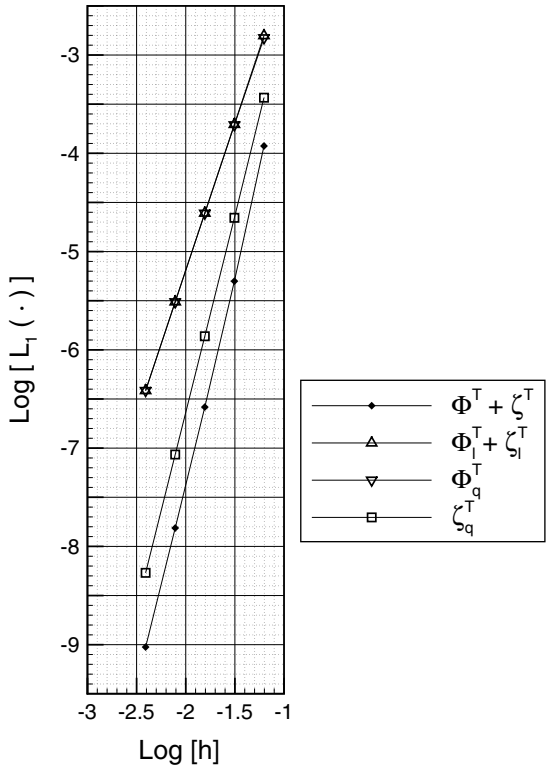

Fig. 6. Mesh-refinement study for the unsteady scalar problem: fluctuation accuracy for the third-order-accurate scheme.

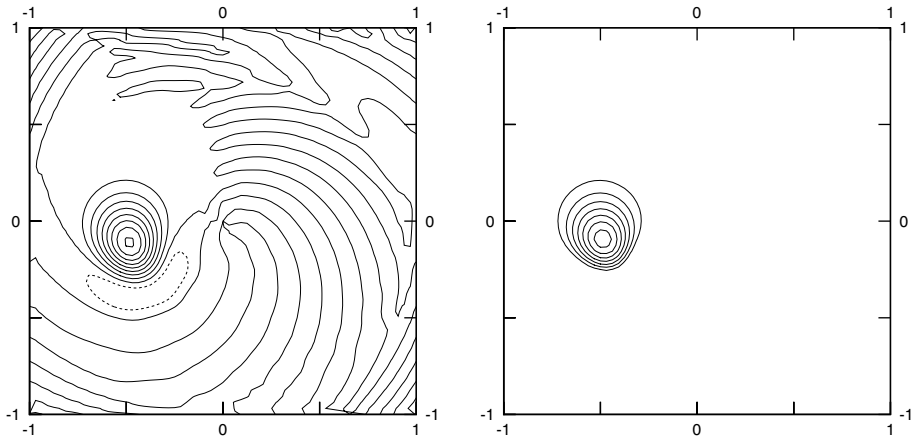

Fig. 7. Rotating hump: Lax–Wendroff explicit scheme solutions; linear (left) and non-linear (right) versions.

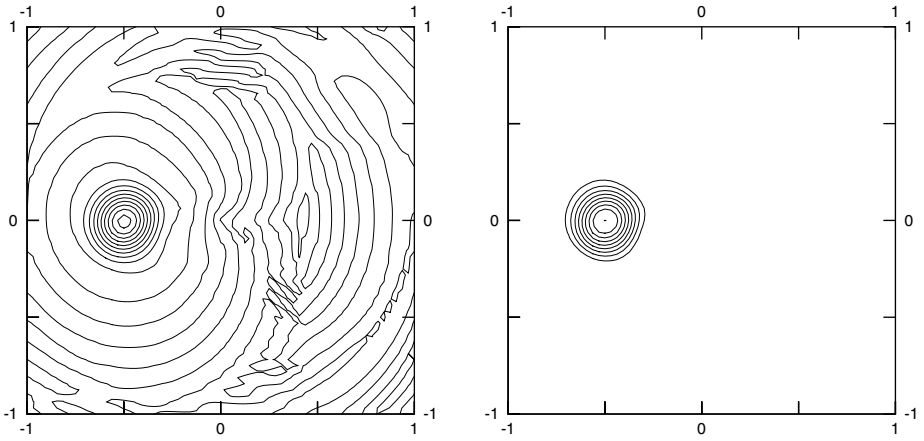

Fig. 8. Rotating hump: solution provided by the second-order-accurate implicit scheme of [18]; linear (left) and non-linear (right) versions.

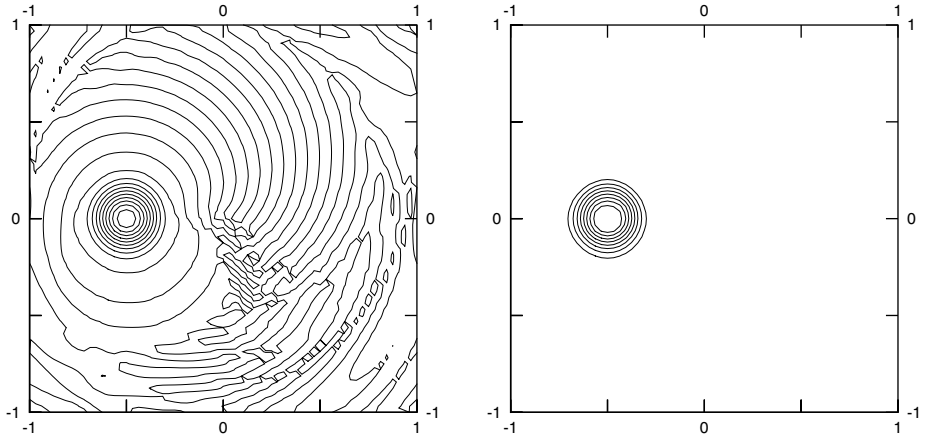

Fig. 9. Rotating hump: solution provided by the third-order-accurate implicit scheme; linear (left) and non-linear (right) versions.

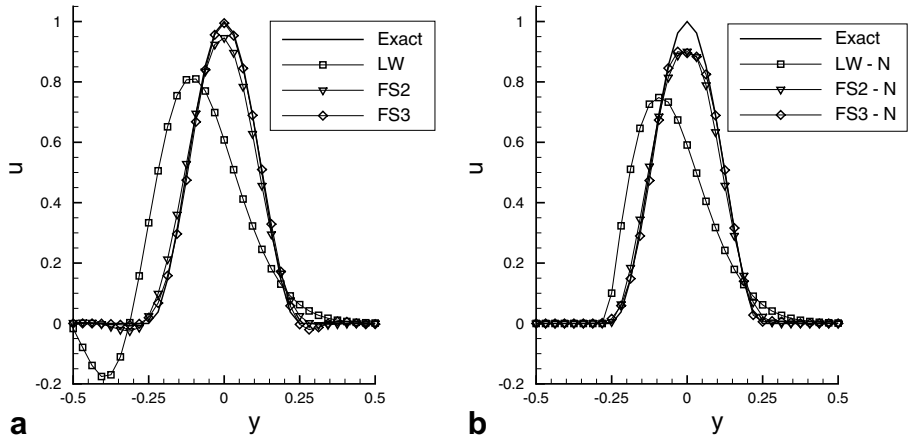

Fig. 10. Comparison between second- and third-order-accurate schemes for the case of a rotating hump: vertical cut at $x = -0.5$, for $t = 1$; linear (left) and non-linear (right) versions.

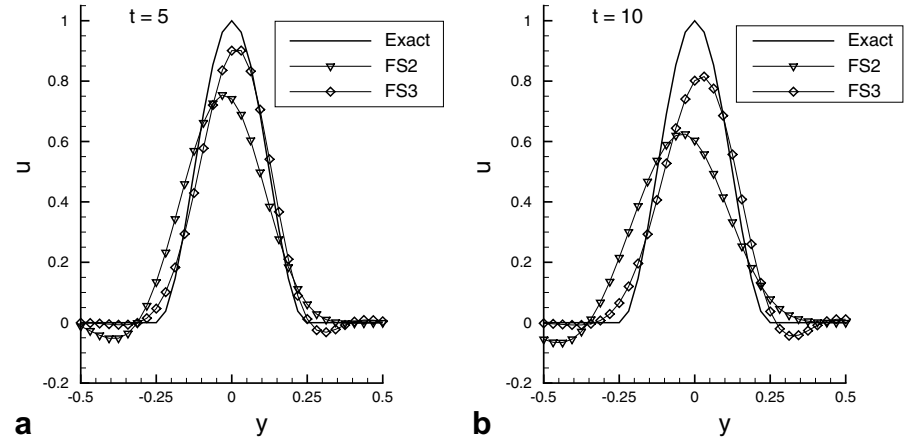

Fig. 11. Comparison between second- and third-order-accurate implicit linear schemes for the case of a rotating hump: vertical cut at $x = -0.5$, after 5 (left) and 10 (right) revolutions (*i.e.*, $t = 5$ and $t = 10$, respectively).

- Fig. 10a and b provide the solutions obtained with the above linear and non-linear schemes, respectively, after one revolution of the hump ($t = 1$);
- Fig. 11a and b provide the solutions after 5 and 10 revolutions, respectively, obtained using the second- and third-order-accurate implicit schemes; the lower numerical errors (both dispersive and diffusive) of the latter scheme are evident.

It is noteworthy that the linear scheme defined with $\alpha_i^T = \beta_i^T$ being unstable, cannot provide any solution for this test case.

3. Euler equations

The extension to systems of conservation laws of the present third-order-accurate implicit scheme is presented. The Euler equations are written in conservative form as

$$\frac{\partial U}{\partial t} = -\frac{\partial F}{\partial x} - \frac{\partial G}{\partial y}, \tag{47}$$

where

$$U = \begin{pmatrix} \rho \\ \rho u \\ \rho v \\ \rho E \end{pmatrix}, \quad F = \begin{pmatrix} \rho u \\ p + \rho u^2 \\ \rho uv \\ \rho uH \end{pmatrix}, \quad G = \begin{pmatrix} \rho v \\ \rho uv \\ p + \rho v^2 \\ \rho vH \end{pmatrix} \tag{48}$$

are the vectors of the conservative variables and of the fluxes in the x and y directions, respectively. In Eq. (48), ρ is the density, p is the pressure, u and v are the Cartesian velocity components, E is the specific total internal energy, and H is the specific total enthalpy.

In order to discretize the system by an FS scheme, Eq. (47) needs to be rewritten in their quasi-linear form:

$$\frac{\partial U}{\partial t} = -\left(A\frac{\partial U}{\partial x} + B\frac{\partial U}{\partial y}\right), \tag{49}$$

where $A = \partial F/\partial U$ and $B = \partial G/\partial U$ are the Jacobian matrices.

The fluctuation over each triangle T is defined as

$$\Phi^T = -\int_T \left(A\frac{\partial U}{\partial x} + B\frac{\partial U}{\partial y}\right) \mathrm{d}S. \tag{50}$$

For a second-order-accurate scheme, a linear variation of the parameter vector $Z = \sqrt{\rho}(1, u, v, H)^{\mathscr{T}}$ over each triangle is assumed; therefore the discrete fluctuation can be evaluated analytically, as

$$\Phi^T = -\left(\overline{A}\overline{\frac{\partial U}{\partial x}} + \overline{B}\overline{\frac{\partial U}{\partial y}}\right)|T|, \tag{51}$$

the bar indicating suitable cell-averaged values [27]. The fluctuation Φ^T is then rewritten in terms of appropriate fluxes through the sides of each triangle (see [28,3], for details) as

$$\Phi^T = -\sum_{j=1}^{3} \frac{\ell_j}{2}\overline{A}\cdot \boldsymbol{n}_j U_j = -\sum_{j=1}^{3} K_j U_j, \tag{52}$$

where

$$K_j = \frac{1}{2}\ell_j(\overline{A}n_{x,j} + \overline{B}n_{y,j}). \tag{53}$$

Due to the hyperbolic nature of the system, K_j can be written as

$$K_j = (\overline{R}_K\overline{\Lambda}_K\overline{L}_K)_j = (\overline{R}_K\overline{\Lambda}_K^+\overline{L}_K)_j + (\overline{R}_K\overline{\Lambda}_K^-\overline{L}_K)_j = K_j^+ + K_j^-. \tag{54}$$

In Eq. (54), $\overline{R}_{K,j}$ and $\overline{L}_{K,j}$ are the right and left eigenvector matrices of K_j, whereas $\overline{\Lambda}_{K,j}^+$ and $\overline{\Lambda}_{K,j}^-$ are the corresponding positive and negative eigenvalue matrices. In such a way, it is possible to provide linear matrix FS schemes for the Euler system, which retain the same properties of the corresponding scalar ones. Introducing the following vector:

$$U_{\mathrm{in}} = \left(\sum_{j=1}^{3} K_j^-\right)^{-1}\left(\sum_{j=1}^{3} K_j^- U_j\right), \tag{55}$$

the linear matrix N scheme [28,3] is obtained as:

$$\Phi_j^N = -K_j^+[U_j - U_{\mathrm{in}}]. \tag{56}$$

The matrix LW scheme does not require any splitting and is simply given as

$$\Phi_j^{\mathrm{LW}} = \left(\frac{1}{3}I + \frac{\Delta t}{2|T|}K_j\right)\Phi^T = \mathbb{B}_i^{T,\mathrm{LW}}\Phi^T. \tag{57}$$

Finally the matrix UCV scheme is given as

$$\Phi_j^{\mathrm{UCV}} = \left[\frac{1}{3}I + \frac{2}{3}\left(\sum_{i=1}^{3}|K_i|\right)^{-1}K_j\right]\Phi^T = \mathbb{B}_i^{T,\mathrm{UCV}}\Phi^T, \tag{58}$$

where $|K_i| = (\overline{R}_K|\overline{\Lambda}_K|\overline{L}_K)_i$.

In order to extend to the Euler system the third-order-accurate scheme described in the previous section, a quadratic variation of the parameter vector, Z, is assumed, by reconstructing the gradient ∇Z_i at each vertex, using Eq. (33). The spacial fluctuation is computed by a contour integral using Simpson's formula

$$\Phi^T = -\sum_{j\in T}\frac{1}{6}[\mathscr{F}(Z_m) + 4\mathscr{F}(Z_{\mathrm{mid},j}) + \mathscr{F}(Z_p)]\cdot\mathbf{n}_j\ell_j,$$

where $\mathscr{F} = (F, G)$ and the notation of Eq. (36) has been employed. The unsteady residual is obtained by integrating over T, namely

$$\Psi^T = \int_T \frac{\partial U}{\partial t}\mathrm{d}S = \frac{|T|}{3}\sum_{j\in T}\left(\frac{\partial U}{\partial t}\right)_{\mathrm{mid},j},$$

where the time derivatives are evaluated using the third-order-accurate backward four-level scheme of Eq. (39).

Finally, the distribution step is accomplished using a *matrix* generalization of the scalar scheme. The dual-time-stepping formulation of the resulting implicit system to be solved is the following:

$$U_i^{n+1,k+1} = U_i^{n+1,k} - \frac{\Delta\tau}{|S_i|}\sum_{T\ni i}(\Psi_i^T + \Phi_i^T)^{n+1,k} = U_i^{n+1,k} - \frac{\Delta\tau}{|S_i|}\sum_{T\ni i}(\mathbb{M}_i^T\Psi^T + \mathbb{B}_i^T\Phi^T)^{n+1,k}$$

with *bounded* distribution matrices $\mathbb{B}_i^T$ and $\mathbb{M}_i^T$. Also in the case of the Euler equations, the choice $\mathbb{M}_i^T = \mathbb{B}_i^T$ leads to a third-order-accurate scheme with poor stability. Therefore, the scalar distribution in Eq. (46) has been generalized to the case of the system as

$$\Psi_i^T + \Phi_i^T = \mathbb{B}_i^T(\Psi_\ell^T + \Phi_\ell^T + \Phi_q^T) + \frac{1}{3}\Psi_q^T. \tag{59}$$

3.1. Results

In this section, numerical results for the Euler equations are discussed; all computations have been performed again using uniform Cartesian grids, the quadrilateral cells being divided into two triangles by alternating diagonals.

Firstly, an accuracy study is performed by computing the advection of a two-dimensional vortex superposed to a uniform flow with $(\rho, u, v, p) = (1, \sqrt{\gamma}, 0, 1)$, with $\gamma = 1.4$. The vortex is given in polar coordinates (r, θ) as:

$$\begin{aligned} u^* &= \epsilon r\,\mathrm{e}^{\alpha(1-\tau^2)}\sin\theta,\\ v^* &= -\epsilon r\,\mathrm{e}^{\alpha(1-\tau^2)}\cos\theta,\\ T^* &= -\frac{(\gamma-1)\epsilon^2}{4\alpha}\mathrm{e}^{2\alpha(1-\tau^2)}, \end{aligned} \tag{60}$$

where $\tau = r/0.05$, $\epsilon = 0.3$, $\alpha = 0.204$, and θ is the counter-clockwise angle, measured with respect to the horizontal direction. Computations have been performed up to $t = 0.2$ in the domain $[0, 2]\times[0, 1]$, using a sequence of five grids, starting from $h = \Delta x = \Delta y = 1/20$ and $\Delta t = 0.0125$, and halving both the space and time steps. In Fig. 12 the scheme is seen to be third-order accurate and it is markedly more accurate than either the FS Lax–Wendroff explicit scheme or the second-order-accurate implicit one of Ref. [18]. The results refer to the linear schemes, since the limiting procedure does not affect the accuracy on sufficiently smooth test cases as verified numerically in [18]. It is noteworthy that, using the third-order-accurate scheme, about 10 inner iterations are needed to reduce the L_∞ norm of the residual of the continuity equation to 10^{-7}.

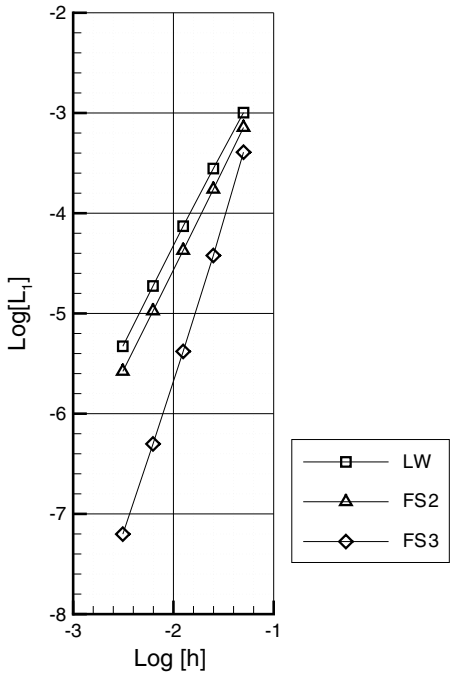

Fig. 12. Accuracy study: vortex advection problem.

Then, the third-order-accurate implicit scheme has been tested, in its non-linear version, versus a severe shock–vortex interaction problem, the results being compared again with those obtained by the second-order-accurate schemes. The interaction between a stationary shock, with upstream conditions $(\rho, u, v, p) = (1, 1.1\sqrt{\gamma}, 0, 1)(M_1 = 1.1)$, and the vortex described in Eq. (60) has been computed in the $[0, 2] \times [0, 1]$ domain using $\Delta x = \Delta y = 1/100$ and $\Delta t = 0.0025$. Figs. 13–15 show the pressure contours at times $t = 0.2$ and $t = 0.4$, obtained using the non-linear LW, FS2, and FS3 schemes, respectively. Due to its low dissipative error, the present third-order-accurate scheme provides a sharp shock-capturing and a well-preserved vortex after the interaction ($t = 0.4$). It is noteworthy that, using the third-order-accurate scheme, about 80 inner iterations are needed to reduce the L_∞ norm of the residual of the continuity equation to 10^{-7}.

Finally, a very severe test case has been considered, namely, the two-dimensional Riemann problem studied in [29]. The initial solution consists of four constant values in four quadrants chosen so that each pair of data gives a single shock wave, the interaction at the corner producing a complex structure, see [29] for details. The problem has been solved in the square domain $[0, 1]^2$ up to the final time $t = 0.8$. Also for this test case, using the third-order-accurate scheme, about 80 inner iterations are needed to reduce the L_∞ norm of the residual of the continuity equation to 10^{-7}. Fig. 16 provides the density contours obtained using the non-linear third-order-accurate scheme on a grid with 100×100 and 200×200 quad-cells, the time step being equal to

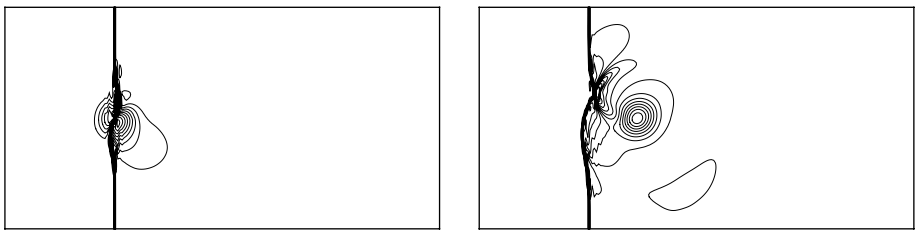

Fig. 13. Shock–vortex interaction: pressure contours ($\Delta p = 0.02$) at $t = 0.2$ (left) and $t = 0.4$ (right); solution provided by the explicit Lax–Wendroff scheme.

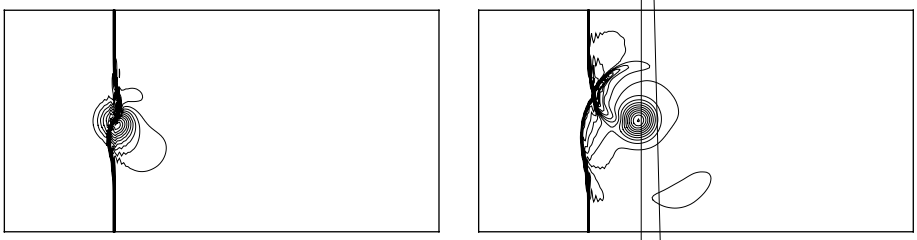

Fig. 14. Shock–vortex interaction: pressure contours ($\Delta p = 0.02$) at $t = 0.2$ (left) and $t = 0.4$ (right); solution provided by the implicit second-order-accurate scheme of [18].

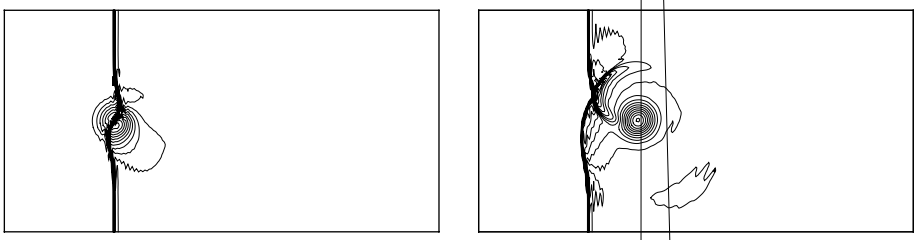

Fig. 15. Shock–vortex interaction: pressure contours ($\Delta p = 0.02$) at $t = 0.2$ (left) and $t = 0.4$ (right); solution provided by the implicit third-order-accurate scheme.

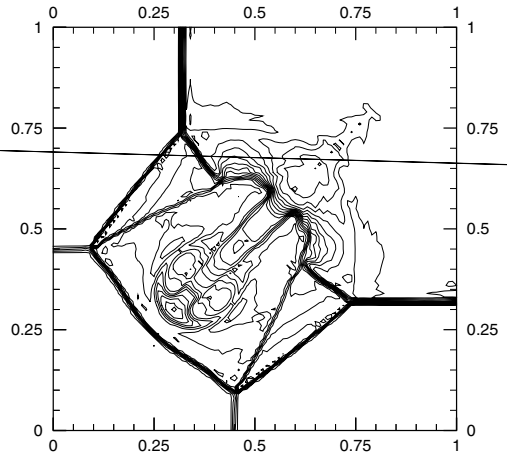

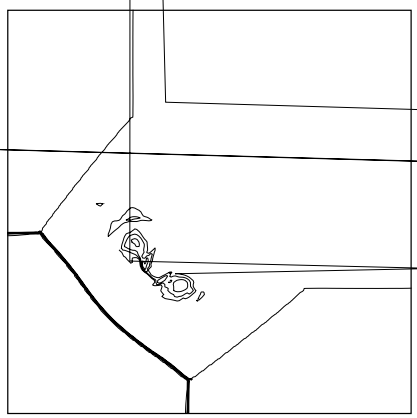

$\Delta t = 0.0032$ and $\Delta t = 0.0016$, respectively. Furthermore, Fig. 17 shows the solutions obtained using the non-linear Lax–Wendroff scheme and the implicit non-linear second-order-accurate scheme (FS2-N) on a 200×200 grid with $\Delta t = 0.0016$ [18]. All schemes provide sharp shocks and contact lines; the Kelvin–Helmholtz instability of the slip lines is captured by the second-order-accurate implicit scheme on the 200×200 grid and by the third-order-accurate implicit scheme already on the coarser 100×100 grid. It is noteworthy that, unlike the previous simpler test case, the lower dissipation of the third-order-accurate scheme causes a remarkable change of the numerical solution with respect to the second-order-accurate scheme. Finally, the robustness of the method is verified by computing the solutions on two refined grids obtained halving twice the space and time intervals, the density contours being given in Fig. 18.

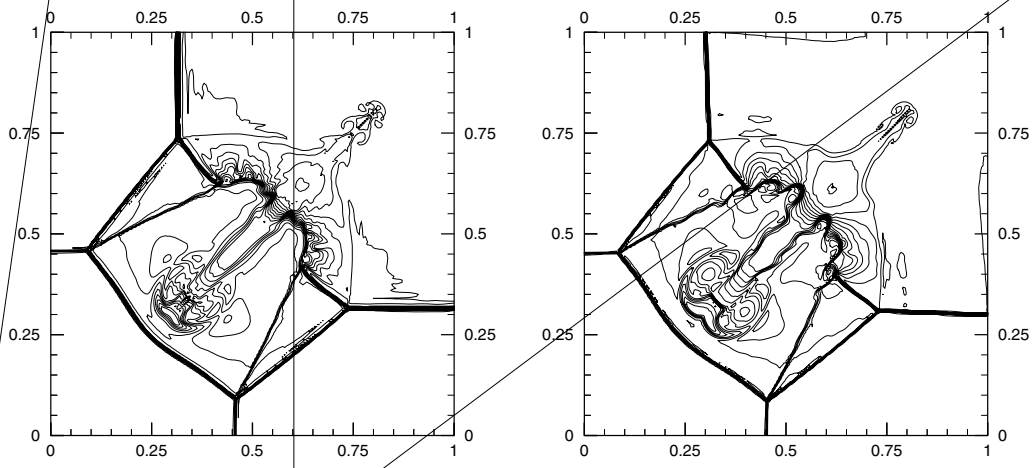

Fig. 17. 2D Riemann problem: density contours ($\Delta\rho = 0.08$) at $t = 0.8$ for the Lax–Wendroff scheme (left) and the FS2-N scheme (right) using a grid with 200×200 quad-cells.

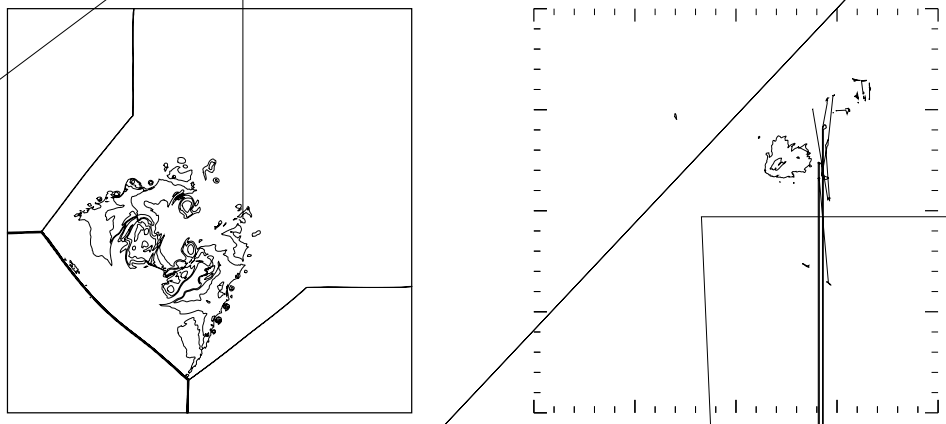

Fig. 18. 2D Riemann problem: density contours ($\Delta\rho = 0.08$) at $t = 0.8$ for the third-order-accurate scheme using a grid with 400×400 (left) and 800×800 (right) quad-cells.

4. Conclusions

This paper provides a higher-order-accurate genuinely multi-dimensional implicit fluctuation splitting scheme for two-dimensional unsteady problems, using a dual-time-stepping approach. A polynomial approximation of the solution over each triangular element, based on the reconstruction of the gradient at the three vertices, is employed together with a suitable finite difference discretization of the time derivative. The sufficient conditions for a stable fluctuation splitting scheme to enjoy a prescribed order of accuracy in both space and time are provided, thus clearing some previous inconsistent findings [16,23,20]. Then, a third-order-accurate fluctuation splitting scheme is proposed for both the scalar advection and the Euler equations, which is stable thanks to an appropriate distribution of the fluctuation in each computational cell and is characterized by very low amplitude and phase errors. When combined with a recently developed limiting procedure, the proposed implicit scheme provides accurate solutions also for very complex discontinuous flow problems.

Acknowledgments

This research has been supported by the MIUR and the Politecnico di Bari, Grant CofinLab 2000 (CEMeC).

Appendix A. Weak formulation of FS schemes

Let us introduce the weak formulation of Eq. (1), which embraces both continuous and discontinuous solutions. Consider the space of $\mathscr{C}_{\mathbf{0}}^{\mathbf{1}}$ functions with compact support in $\mathbb{R}^2 \times [0, \infty[$; for any scalar function $\varphi \in \mathscr{C}_{\mathbf{0}}^{\mathbf{1}}$, one has:

$$\int_0^{+\infty} \int_{\mathbb{R}^2} \left[\frac{\partial u}{\partial t} + \nabla \cdot \mathbf{F} \right] \varphi \, \mathrm{d}\Omega \, \mathrm{d}t = 0. \tag{A.1}$$

The explicit updating formula (4) for an FS scheme can be derived starting from Eq. (A.1) considering for each node i a function $\varphi(\mathbf{x}, t) = \ell(t)\omega_i(\mathbf{x})$, with $\ell(t) = 1$ in the interval $[t, t + \Delta t]$, otherwise $\ell(t) = 0$. Eq. (A.1) is rewritten as

$$\int_t^{t+\Delta t} \sum_{T \ni i} \int_T \left[\frac{\partial u}{\partial t} + \nabla \cdot \mathbf{F} \right] \omega_i^T \, \mathrm{d}\Omega \, \mathrm{d}t = 0, \tag{A.2}$$

where ω_i^T is the restriction of ω_i to the triangle T. Therefore, one has

$$\sum_{T \ni i} \int_T \omega_i^T \int_t^{t+\Delta t} \frac{\partial u}{\partial t} \mathrm{d}t \, \mathrm{d}\Omega + \sum_{T \ni i} \int_t^{t+\Delta t} \int_T \omega_i^T \nabla \cdot \mathbf{F} \, \mathrm{d}\Omega \, \mathrm{d}t = 0. \tag{A.3}$$

The steady term at the left-hand side of Eq. (A.3) is written as

$$\sum_{T \ni i} \int_t^{t+\Delta t} \phi_i^T(t) \, \mathrm{d}t = \Delta t \sum_{T \ni i} \phi_i^{T,n}, \tag{A.4}$$

where an explicit integration with $\phi_i^T(t) = \phi_i^{T,n}$ has been chosen, and the signal to node i is defined as

$$\phi_i^{T,n} = \int_T \omega_i^T \nabla \cdot \mathbf{F}(u^n) \, \mathrm{d}\Omega. \tag{A.5}$$

Since for an FS scheme one has

$$\sum_{j \in T} \phi_j^T = \phi^T = \int_T \nabla \cdot \mathbf{F} \, \mathrm{d}\Omega, \tag{A.6}$$

the following condition must be satisfied by the weight functions over each element:

$$\sum_{j \in T} \omega_j^T(\mathbf{x}) = 1. \tag{A.7}$$

The first term at the left-hand side of Eq. (A.3) is computed as

$$\sum_{T \ni i} \int_T [u^{n+1} - u^n] \omega_i^T \mathrm{d}\Omega = [u_i^{n+1} - u_i^n] \sum_{T \ni i} \int_T \omega_i^T \mathrm{d}\Omega = [u_i^{n+1} - u_i^n] |S_i|, \tag{A.8}$$

where

$$|S_i| = \sum_{T \ni i} \int_T \omega_i^T \, \mathrm{d}\Omega,$$

is the area of the dual cell, and the nodal values u_i^n and u_i^{n+1} are assumed to represent the averages over the dual cell, S_i. Finally, substituting Eqs. (A.4) and (A.8) in Eq. (A.3), the standard updating formula (4) for an FS scheme is recovered.

References

[1] R. Struijs, H. Deconinck, P.L. Roe, Fluctuation Splitting Schemes for the 2D Euler Equations, VKI LS 1991-01Computational Fluid Dynamics, von Karman Institute, Belgium, 1991.

[2] E. van der Weide, H. Deconinck, E. Issmann, G. Degrez, Fluctuation splitting schemes for multidimensional convection problems: an alternative to finite volume and finite element methods, Comput. Mech. 23 (1999) 199.

[3] P. De Palma, G. Pascazio, M. Napolitano, A hybrid fluctuation splitting scheme for two-dimensional compressible steady flows, in: M.M. Hafez, J.J. Chattot (Eds.), Innovative Methods for Numerical Solution of Partial Differential Equations, World Scientific Publishing Co. Inc., New Jersey, 2002, pp. 305–333.

[4] R. Abgrall, M. Mezine, Construction of second-order accurate monotone and stable residual distribution schemes for steady problems, J. Comput. Phys. 195 (2004) 474.

[5] H. Deconinck, R. Struijs, H. Paillère, L.A. Catalano, P. De Palma, M. Napolitano, G. Pascazio, Development of cell-vertex multidimensional upwind solvers for the compressible flow equations, CWI Quart. 6 (1993) 1.

[6] L.A. Catalano, P. De Palma, G. Pascazio, M. Napolitano, Cell-vertex adaptive Euler method for cascade flows, AIAA J. 33 (1995) 2299.

[7] E. van der Weide, H. Deconinck, Positive matrix distribution schemes for hyperbolic systems, in: Computational Fluid Dynamics '96, 1996, pp. 747–753.

[8] A. Bonfiglioli, P. De Palma, G. Pascazio, M. Napolitano, An implicit fluctuation splitting scheme for turbomachinery flows, ASME J. Turbomach. 127 (2005) 395.

[9] C.-S. Chou, C.-W. Shu, High order residual distribution conservative finite difference WENO schemes for steady problems on non-smooth meshes, J. Comput. Phys. 214 (2006) 698.

[10] R. Abgrall, F. Marpeau, Residual distribution schemes on quadrilateral meshes, J. Sci. Comput. (2006), doi:10.1007/s10915.005.9023.2.

[11] P. De Palma, G. Pascazio, D.T. Rubino, M. Napolitano, Residual distribution schemes for advection and advection–diffusion problems on quadrilateral cells, J. Comput. Phys. (2006), doi:10.1016/j.jcp.2006.02.003.

[12] J. März, G. Degrez, Improving time accuracy for residual distribution schemes, von Karman Institute Project Report 1996-17, 1996.

[13] A. Ferrante, H. Deconinck, Solution of the unsteady Euler equations using residual distribution and flux corrected transport, von Karman Institute Project Report 1997-08, 1997.

[14] M.E. Hubbard, P.L. Roe, Compact high resolution algorithms for time dependent advection problems on unstructured grids, Int. J. Numer. Methods Fluids 33 (2000) 711.

[15] Á. Csík, M. Ricchiuto, H. Deconinck, S. Poedts, Space–time residual distribution schemes for hyperbolic conservation laws, AIAA Paper 2001-2617, 2001.

[16] R. Abgrall, M. Mezine, Construction of second order accurate monotone and stable residual distribution schemes for unsteady flow problems, J. Comput. Phys. 188 (2003) 16.

[17] R. Lohner, K. Morgan, M. Vahadati, J.P. Boris, D.L. Book, FEM-FCT: combining unstructured grids with high resolution, Commun. Appl. Numer. Methods 4 (1988) 717.

[18] P. De Palma, G. Pascazio, G. Rossiello, M. Napolitano, A second-order-accurate monotone implicit fluctuation splitting scheme for unsteady problems, J. Comput. Phys. 208 (2005) 1.

[19] R. Abgrall, P.L. Roe, High order fluctuation schemes on triangular meshes, J. Sci. Comput. 19 (2003) 3.

[20] R. Abgrall, Construction of High-Order Residual Distribution Schemes for Scalar Problems. Preliminary results for systems, VKI LS 2006-01CFD-Higher Order Discretization Methods, von Karman Institute, Belgium, 2005.

[21] D. Caraeni, L. Fuchs, Compact third-order multidimensional upwind scheme for Navier–Stokes simulations, Theor. Comput. Fluid Dynam. 15 (2002) 373.

[22] D. Caraeni, L. Fuchs, Compact third-order multidimensional upwind discretization for steady and unsteady flow simulations, Comput. Fluids 34 (2005) 419.

[23] R. Abgrall, N. Andrianov, M. Mezine, Towards very high-order accurate schemes for unsteady convection problems on unstructured meshes, Int. J. Numer. Methods Fluids 47 (2005) 679.

[24] H. Paillère, Multidimensional upwind residual distribution schemes for the Euler and Navier–Stokes equations on unstructured grids. Ph.D. Thesis, Université Libre de Bruxelles, Belgium, 1995.

[25] M. Ricchiuto, N. Villedieu, R. Abgrall, H. Deconinck, High-order Residual Distribution Schemes: Discontinuity Capturing Crosswind Dissipation and Extension to Advection–Diffusion. VKI LS 2006-01CFD-Higher Order Discretization Methods, von Karman Institute, Belgium, 2005.

[26] A. Jameson, Time dependent calculations using multigrid with applications to unsteady flows past airfoils and wings, AIAA Paper 91-1596, 1991.

[27] H. Deconinck, P.L. Roe, R. Struijs, A multidimensional generalization of Roe's flux difference splitter for the Euler equations, Comput. Fluids 22 (1993) 215.

[28] E. van der Weide, H. Deconinck, Positive matrix distribution schemes for hyperbolic systems, with applications to the Euler equationsComputational Fluid Dynamics '96, Wiley, New York, 1996, pp. 747–753.

[29] R.J. Le Veque, Wave propagation algorithms for multidimensional hyperbolic systems, J. Comput. Phys. 131 (1997) 327.